Effect of Molecular Weight on Hydrated Morphologies of the Short-Side-Chain Perfluorosulfonic Acid Membrane

Dongsheng Wu,[†] Stephen J. Paddison,*[,†] and James A. Elliott[‡]

Department of Chemical and Biomolecular Engineering, University of Tennessee, Knoxville, Tennessee 37996, and Department of Materials Science and Metallurgy, University of Cambridge, Pembroke Street, Cambridge, CB2 3QZ, U.K.

Received January 5, 2009; Revised Manuscript Received March 30, 2009

ABSTRACT: We have carried out dissipative particle dynamics (DPD) simulations in an attempt to better understand how molecular weight (MW) affects the hydrated morphology of the short-side-chain (SSC) perfluorosulfonic acid (PFSA) fuel cell membrane. Previously, we demonstrated that such coarse-grained simulations are capable of revealing differences in the morphology of PFSA membranes when either the length of the side chain or equivalent weight (EW) of the ionomer is changed [Wu et al. *Energy Environ. Sci.* 2008, *1*, 284−293]. In the present investigation, the SSC ionomer was modeled using macromolecules of the ionomer with EWs of 753, 798 and 849, each at three distinct MWs. The morphological structures were then investigated as a function of EW, MW and degree of hydration (with water contents corresponding to $\lambda = 5$, 7, 9, 11, and 16 H_2Os/SO_3H). Water contour plots reveal that the isolated water clusters present at lower water contents increase in size with increasing levels of hydration, and eventually form continuous water domains. The increase of MW induces aggregation of the fluorocarbon backbone in order to minimize chain bending forces while maintaining a phase-separated structure, and results in larger, more elongated water domains, especially at high EWs. Furthermore, the Bragg spacing corresponding to periodicity of water domains, computed from radial distribution functions (RDFs), shows that the spacing between water domains increases with increasing hydration levels. This occurs especially for higher MW polymers at high hydration (16 H_2Os/SO_3H), whereas there is little difference at lower hydration levels between polymers with different MW.

Introduction

Efficient generation of power accompanied by minimal pollution for diverse applications such as transportation, residential, and portable devices has spurred the research and development of proton exchange membrane (PEM) fuel cells. The critically important electrolyte serves not only as a separator of the electrodes and reactant gases but also as the medium through which protons are transported (anode to cathode) and with the external flow of electrons (also anode to cathode) complete the electrical circuit. Efficient operation of the device is dependent on not only the choice of the components (e.g., catalysts, electrolyte, etc) but also their chemical structure and morphology along with the interfaces between the components. The harsh operating conditions (high temperature, presence of highly reactive oxidizing radicals, etc) of PEM fuel cells demand that the electrolyte exhibit hydrolytic, thermo-oxidative, and electrochemical stability. The advantages (i.e., increase in catalytic and transport rates and resistance to CO poisoning at the anode) of high temperature operation ($T > 100$ °C) accompanied with little humidification have driven the development of novel high performance electrolytes and the desire to understand how structure and hydrated morphology determine proton conductivity in existing PEMs.[1]

Perfluorinated ionomers are a widely utilized electrolyte in PEM fuel cells functioning not only as the conductor of protons but also as a separator of the electrodes and fuel gases. The archetypal electrolyte is Nafion, a perfluorosulfonic acid (PFSA) membrane,[2] that has been subject to extensive study of its morphology, structure and transport properties.[3] Although Nafion exhibits many desirable qualities for fuel cell applications, and is still a popular material, it still has serious limitations such as a restrictive range of thermal stability, high manufacturing cost and the requirement of a significant level of hydration in order to exhibit sufficient proton conductivity (i.e., ≥0.1 S/cm).[4] Therefore, the search for novel membrane materials with superior properties has been actively pursued in fuel cell research, and has resulted in the synthesis and development of a whole range of diverse materials[5] including various chemical homologues of Nafion.

The short-side-chain (SSC) PFSA membrane,[6−19] originally synthesized by Dow Chemical[20] and now commercialized by Solvay Solexis as Hyflon,[12,14] contains a shorter side chain, $-OCF_2CF_2SO_3H$, as compared to that of Nafion (i.e., $-OCF_2CF(CF_3)OCF_2CF_2SO_3H$), attached to a polytetrafluoroethylene (PTFE) backbone. Although the original SSC PFSA membranes showed some improved properties[21−23] and enhanced performance in a fuel cell,[9] they did not see widespread application due to a complex synthesis process. However, with the much simpler synthesis route recently developed by Solvay Solexis, the SSC PFSA membrane has attracted increasing attention.

The earlier comprehensive work by Tant et al.[6,7] and Moore and Martin[8] on SSC PFSA membranes with different equivalent weight (EW), which corresponds to the number of grams of dry ionomer per mole of sulfonic acid, have highlighted property differences when compared to Nafion. Their most significant results demonstrate that the SSC PFSA membranes have higher crystallinity at similar EWs and a higher glass transition temperature (T_g) thereby allowing a wider range of operating temperatures for implementation as the electrolyte in fuel cells, potentially important for automotive applications. The increase in water uptake with decreasing EW has also been evaluated and attributed to the lower crystallinity at lower EWs.[8] Recently, the conductivity and hydrogen permeability of SSC PFSA membranes have been reported in subfreezing conditions, and

* Author to whom correspondence should be addressed. E-mail: spaddison@utk.edu.
[†] Department of Chemical and Biomolecular Engineering, University of Tennessee.
[‡] Department of Materials Science and Metallurgy, University of Cambridge.

10.1021/ma900016w CCC: $40.75
Published on Web 04/15/2009

remarkable durability of fuel cells employing these membranes has also been demonstrated.[16] An investigation into the chemical degradation of SSC PFSA membranes revealed that temperature has a negligible effect on degradation while reactant humidification has a large influence.[15] Recent work by Kreuer et al.[17] has attempted to establish the relationship between performance and other properties by investigating the SSC PFSA membranes from a broad perspective including water sorption, proton and water transport, microstructure, and visco-elastic properties. This study demonstrated, in comparison to Nafion, that the combination of high ion exchange capacity (IEC) and high mechanical stability of the SSC ionomer may offer better performance in PEM fuel cells.

X-ray and neutron scattering technologies have been widely utilized to probe the hydrated morphology of PFSA membranes. In addition to wide-angle X-ray scattering (WAXS) to study the crystallinity of SSC PFSA membranes, Moore and Martin used small-angle X-ray scattering (SAXS) to demonstrate the size of ionic clusters based on a hard-sphere interference model.[8,24] Later, Gebel and Moore carried out a further structural studies on dry and water-swollen SSC PFSA membranes with SAXS and SANS experiments.[11] The detailed crystalline contribution was studied from the scattering data based on a local order model.[25] Kreuer has also undertaken SAXS studies on SSC PFSA membranes and Nafion at various hydration levels and showed that the SSC ionomer exhibits higher rigidity when compared to Nafion.[17]

There are a number of different models in the literature which have been proposed to interpret the scattering data of Nafion. The original cluster-network model proposed by Gierke et al. has been the most widely referenced model in the history of PFSA ionomers.[26–28] Following this early work, a host of additional models were developed including: the modified (depleted-zone) core−shell proposed by Fujimura et al.,[29] a lamellar model proposed by Litt,[30] a sandwich-like model proposed by Haubold et al.,[31] a fibrillar model proposed by Rubatat et al.,[32] a channel model by Kreuer,[33] and most recently a parallel cylindrical channel model by Schmidt-Rohr.[34] These various models have provided a framework for understanding the morphologies of hydrated PFSA membranes determined from experimental work, but are still lacking molecular level details due to the complexity of the studied morphologies.

Multiscale computational efforts have contributed to a better understanding of structures on the molecular scale, as well as larger scale morphological structures and chemical functionalities of PFSA membranes and much of this work using a variety of different simulation techniques has been reviewed by several authors.[35–37] *Ab initio* electronic structure calculations, concerning the effects of structure and local chemistry on proton dissociation and exchange at hydrated side chains, have been undertaken on oligomeric fragments of SSC PFSA membranes with a few explicit water molecules giving hydration levels of up to $3H_2O/SO_3H$.[38–41] Furthermore, *ab initio* molecular dynamics (AIMD) calculations have also been performed to investigate proton transfer and dynamics under conditions of high density of perfluorinated sulfonic acid groups.[42–45] On a larger scale are the classical molecular dynamics (MD) simulations on structural correlations and transport properties of PEMs.[46–56] These include empirical valence bond (EVB) models of the solvation and transport of hydrated protons.[57,58] To examine length and time scales that are several orders of magnitude greater and longer than atomistic simulations, it is necessary to perform coarse-grained modeling.[59–63] Mesoscale modeling involving dissipative particle dynamics (DPD) simulations has been employed to study the modeling morphology evolution of a wide range of copolymer systems, including ionomers, during phase separation.[62,64–69] Yamamoto and Hyodo[62] used DPD simulations to investigate the mesoscopic structure of Nafion membranes at varying degrees of hydration. Self-consistent mean-field (SCMF) simulations have been used to study phase separation, and morphological changes in PEMs as a function of temperature and water content.[59] For example, a recent mesoscale simulation on the morphology of hydrated PFSA membranes analogous to Nafion 117 has been carried out by Wescott et al.,[61] using MESODYN code, which is based on a mean-field free energy functional approach. Finally, the present authors performed a comparative study of the hydrated morphologies of three PFSA ionomers with side chains of different length using DPD simulations.[68]

In the present work, we have carried out DPD simulations to investigate the morphology of the SSC PFSA ionomer as a function of water content at three different EWs and molecular weights (MWs). EWs of 753, 798, and 849 were selected because they are located in an interesting range such that real membranes possess good mechanical properties due to a high level of crystallinity and a degree of hydration sufficient to provide high proton conductivity.[7,8] It should be noted that the 850 EW SSC PFSA membrane has a similar crystallinity level and comparable mechanical properties to 1100 EW Nafion.[12] A series of polymers with varying MWs have been created at each EW, and used to systematically study the influence of MW on the model morphologies. Although we are not aware of any published experimental studies detailing MWs for SSC PFSAs, the largest MWs considered in our current study correspond approximately to the lower end of the generally accepted range of MWs for Nafion (between 10^5 and 10^6 g mol^{-1}).[3] This should be compared with some previous MD[47] and DPD[62] studies of Nafion, which used molecules with MWs at least 1 order of magnitude lower. Intermediate hydration levels were selected corresponding to water contents of: 5, 7, 9, 11, and 16 H_2O/SO_3H. The SSC PFSA polymer molecules in the DPD simulations were modeled by connecting soft spherical particles or "beads", which represent groups of several atoms. It is important to note that, since soft potential interactions were used, it is impossible to prevent chain crossing events, and hence the effect of chain entanglements cannot be taken into account. Water was also modeled as a collection of several water molecules. Flory−Huggins χ-parameters were calculated for each coarse-grained particle based on optimized structures and further used to derive the corresponding interaction parameters for the DPD simulations. The radial distribution functions (RDFs) of water particles were generated from DPD calculated densities and used to characterize the water clusters and their average sizes. Finally, the scattering intensities have also been calculated according to the Fourier transform of RDFs, and later used to evaluate the average spacing between water clusters.

The remainder of the paper is structured as follows. First, we briefly review the theoretical background of the DPD method, and describe in detail the coarse-grained models used for SSC polymer molecules. We then outline the procedure for calculating DPD interaction parameters and how to calculate radial distribution functions and simulated scattering intensities from the resulting models. The results are divided into two sections: the first describing the phase segregated morphology of SSC PFSA systems qualitatively using 3D and 2D density maps, and the second containing a quantitative structural analysis of the morphologies based on radial distribution functions and simulated scattering.

Model and Theoretical Methodology

I. DPD Simulations and Model for Short-Side-Chain Perfluorosulfonic Acid Membranes. The DPD method was introduced by Hoogerbrugge and Koelman for simulating complex hydrodynamic behavior of isothermal fluids,[70,71] and

further developed by Español who included stochastic differential equations and conservation of energy.[73,74] In general, the interaction between two DPD particles can be expressed as the sum of a conservative force $\mathbf{F}_{ij}^{C}$, a dissipative force $\mathbf{F}_{ij}^{D}$, a random force $\mathbf{F}_{ij}^{R}$ and a harmonic spring force $\mathbf{F}_{ij}^{S}$ for the system:

$$\mathbf{f}_i = \sum_{j \neq i} (\mathbf{F}_{ij}^{C} + \mathbf{F}_{ij}^{D} + \mathbf{F}_{ij}^{R} + \mathbf{F}_{ij}^{S}) \quad (1)$$

The positions and velocities of the DPD particles are solved in accordance to the above equations by implementing Newton's equation of motion and a modified version of the velocity−Verlet algorithm,[64] as implemented in the Materials Studio software package.[72] The conservative force is derived from a potential exerted on particle i by the jth particle,[64] and it is treated as a soft repulsion action along the line of centers with the form[65,66]

$$\mathbf{F}_{ij}^{C} = \begin{cases} -a_{ij}(r_c - r_{ij})\mathbf{n}_{ij} & r_{ij} < r_c \\ 0 & r_{ij} \geq r_c \end{cases} \quad (2)$$

where a_{ij} is a maximum repulsion force between particle i and j, r_c is a selected cutoff radius of the interaction, $\mathbf{r}_{ij} = \mathbf{r}_i - \mathbf{r}_j$, $r_{ij} = |\mathbf{r}_{ij}|$, and $\mathbf{n}_{ij} = \mathbf{r}_{ij}/|\mathbf{r}_{ij}|$. The repulsive interaction parameters a_{ij} required for the calculation of conservative forces are related to the Flory−Huggins χ-parameter as follows:[64,65]

$$a_{ij} = a_{ii} + 3.27\chi \quad (3)$$

Here a_{ii} is the repulsion parameter between particles of the same type and has the value of $25k_BT$, which gives a pure DPD fluid with compressibility similar to that of liquid water. The general expression, in the Flory−Huggins model, for the free energy of mixing in a binary system is:

$$\frac{\Delta G}{RT} = \frac{\varphi_1}{x_1}\ln \varphi_1 + \frac{\varphi_2}{x_2}\ln \varphi_2 + \chi\varphi_1\varphi_2 \quad (4)$$

where ΔG is the free energy of mixing per mole of lattice site, and ϕ_i is the volume fraction and x_i the degree of polymerization of the ith component. The χ parameter is defined as

$$\chi = z\Delta w_{12}/RT \quad (5)$$

where z is the coordination number of the model lattice and Δw_{12} is the energy of formation of an unlike pair and defined as:

$$\Delta w_{12} = w_{12} - \frac{1}{2}(w_{11} + w_{22}) \quad (6)$$

where w_{ij} is the energy of a particular ij pair. Further details can be found in the work by Fan et al.[75] and Schweizer and Curro.[76] When two components do not favor contact, the parameter χ is positive; when they favor each other, the value of the parameter will be small and even negative. With the polymer length N taken into account, the product χN is important in determining the phase separation of simple polymer−polymer or polymer−solvent mixtures.[64]

The general molecular structure of the SSC PFSA membrane is shown in Figure 1. With $x = 9$ and $y = 15$ chosen in this work, the m and n values are varied to construct SSC PFSA ionomers with a distribution in the spacing of the side chains along the PTFE backbone with average EWs of 753, 798, and 849 g/mol. For example, $m = 3$ and $n = 4$ will give an average EW of 753. By varying the value of p, a range of MWs can be generated. In this way, we constructed MWs of 9036, 18072, and 36144 for an EW of 753, MWs of 11970, 23940, and 47880 for an EW of 798, and MWs of 17838, 35676, and 71352 g/mol for an EW of 849, respectively. The polymer is modeled by connecting spherical soft particles (beads), which contain groups of atoms and/or molecules. The ionomer consists of three distinct DPD beads in all simulations, denoted *A*, *B* and *C*, which correspond to $-CF_2CF_2CF_2CF_2$-CF_2CF_2-, $-CF_2CF_2CF_2CF(OCF_3)-$ and $-CF_2SO_3H\cdot 3H_2O$, respectively. We chose to include the water molecules of the first hydration sphere of the terminal sulfonic acid group in the *C* bead as our interest in the SSC ionomer is due to its higher proton conductivity at intermediate hydration levels. Another independent water particle, denoted *W*, was constructed from six water molecules. The structures of particles *A*, *B*, and *W* were optimized using molecular mechanics with COMPASS parameters using the Forcite module in Materials Studio.[72] The particles *A* and *B* are taken as repeat units in the polymer for the optimizations. The structure of particle *C* was optimized using electronic structure calculations employing the B3LYP hybrid density functional and the 6-31G** basis set with Gaussian 03.[77] The Flory−Huggins χ-parameters were then calculated at room temperature with COMPASS force field parameters by using the Blends module in Materials Studio and the computed repulsion parameters are listed in Table 1.

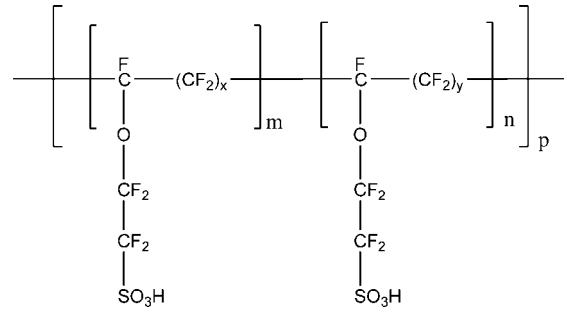

Figure 1. General molecular structure of the macromolecules of the SSC PFSA acid ionomer used in the simulations. Distinct x and y values give different spacing of the side chains within the same macromolecule, selection of m and n determine the EW, and the value of p determines the MW of the ionomer.

Table 1. Computed χ-Parameters and Corresponding Repulsion Parameters Describing Pair Wise Interactions for the Selected Beads of SSC PFSA Ionomer

pair[a]	χ	a_{ij} (k_BT)
A−B	0.15	25.5
A−C	6.86	47.4
A−W	3.28	35.7
B−*C*	6.24	45.4
B−W	3.15	35.3
C−W	1.24	29.0

[a] DPD beads in pairs are as follows: A, $-CF_2CF_2CF_2CF_2CF_2CF_2-$; B, $-CF_2CF_2CF_2CF(OCF_3)-$; C, $CF_3SO_3H\cdot 3H_2O$; W, $6H_2O$.

A simulation box size of 40 × 40 × 40 was selected for our DPD simulations, which resulted in 192000 DPD particles according to the density $\rho = 3$. The spring constant, C, was set to the default value of $4.0k_BT$ from the DPD module in Materials Studio. Following the method of Groot and Rabone,[66] the interaction radius r_c was determined to be about 8.14 Å, and the simulated time step was about 5.35 ps.[68]

II. Generation of RDFs and Bragg Spacing Calculations. While the DPD simulation generates the densities of beads on lattice sites, the distributions of beads about a lattice point P is assumed to have a Gaussian form[78]

$$D_p(r) = \frac{N}{(2\pi\sigma^2)^{3/2}}\exp\left(-\frac{r^2}{2\sigma^2}\right) \quad (7)$$

in which r is the distance from a reference lattice point, N is the number density on the reference lattice point, and σ is a standard distance. When considering the distribution of beads on a certain lattice point other than the reference lattice point, a more useful asymmetric distribution function will be given by

$$D(r) = \frac{N}{(2\pi)^{1/2}\sigma}\frac{r}{r_p}\left[\exp\left(-\frac{(r-r_p)^2}{2\sigma^2}\right) - \exp\left(-\frac{(r+r_p)^2}{2\sigma^2}\right)\right] \quad (8)$$

where r_p is the distance from a lattice point P to the reference lattice point N. By summing distributions from all the lattice points around the reference lattice point, we obtain:[68]

$$4\pi r^2 n g(r) = \frac{r}{(2\pi)^{1/2}}\sum_i \frac{N_i}{r_i\sigma_i}\left[\exp\left(-\frac{(r-r_i)^2}{2\sigma^2}\right) - \exp\left(-\frac{(r+r_i)^2}{2\sigma^2}\right)\right] \quad (9)$$

where n is the average number density, and $g(r)$ is the radial distribution function.

The scattering intensities $I(Q)$ were related to the radial distribution function $g(r)$ by Fourier transformation for our finite-sized system,[79,80] according to

$$I(Q,R) \equiv 4\pi\rho\int_0^R dr r^2\left[\frac{\sin(Qr)}{Qr}\right][g(r)-1] \quad (10)$$

where Q is the magnitude of the scattering vector and ρ is the average density over all space. The physical dimension or Bragg spacing (d) associated with the first peak at the maximum small angle scattering vector Q_m was then evaluated from the Bragg relationship, $d = 2\pi/Q_m$.

Results and Discussion

I. Morphology of Phase Segregated SSC PFSA systems. Figure 2 shows the hydrated morphologies of SSC PFSA systems, with dimensions of 32.4 nm cubed (i.e., 32.4 × 32.4 × 32.4 nm^3), over a range of hydration levels (λ = 5, 7, 11, and 16 H_2O/SO_3H) at fixed EW = 753 and a MW = 18072 g/mol. The three-dimensional (3D) images show the distribution of fluorocarbon beads (A, B) in red, terminal ionic side group beads (C) in green and water beads (W) in blue, after 5.35 ns of equilibration. By visual inspection of Figure 2a−c, it can be seen that as the hydration level is increased, distinct clustering of the C and W beads is first observed for $\lambda = 7$, followed by partial coalescence and percolation of the clusters at $\lambda = 11$. It is evident (from Figure 2d) that long-range connectivity of the water domains occurs at the highest water content ($\lambda = 16$).

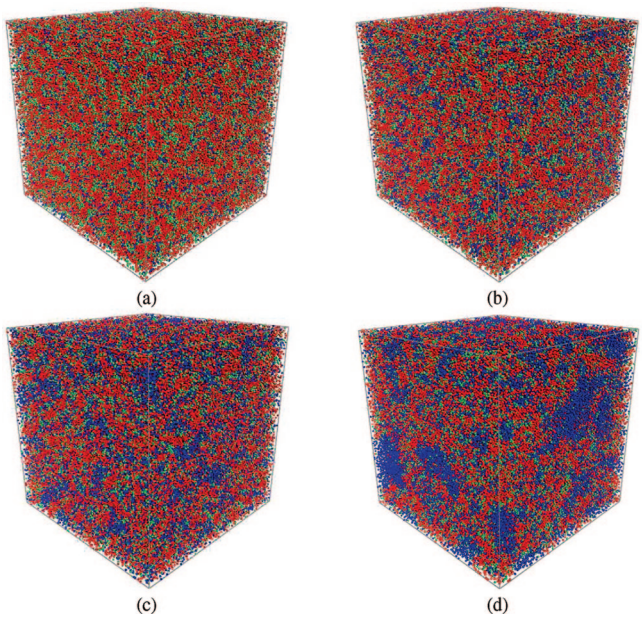

Figure 2. The simulation box showing the hydrated morphologies of the SSC PFSA ionomer with an EW = 753 and MW = 18072 g/mol at water contents of: (a) 5; (b) 7; (c) 11; and (d) 16 H_2O/SO_3^-. A and B beads shown in red, C beads in green, and W beads in blue.

This behavior is broadly consistent with that observed in previous simulation studies at both the molecular[39–42] and mesoscale level,[62,68] and supports the concept of the locally isolated water and ion-clustered morphology at the lower water contents as suggested by Hsu and Gierke,[27,28] but a more channel morphology as the water is increased.[33] However, it is difficult to draw any firm conclusions by visual inspection of the 3D structures alone, and so further qualitative and quantitative analysis was performed.

Figure 3 shows contour plots of the density of water (W) beads in two-dimensional (2D) cross sections for the corresponding 3D models shown in Figure 2. The 2D slices were calculated by averaging the projection of water density onto the planes parallel to the first and second axes, and the darkness of the gray level is linearly proportional to the water density over the range from 0.00 to 3.25. A visual inspection of parts a−d of Figure 3 confirms the observations from Figure 2 that the water clusters are disconnected for $\lambda = 5$ and $\lambda = 7$, partially connected for $\lambda = 11$, and fully percolating for $\lambda = 16$. The precise point percolation or 'full connectivity' occurs is now inferable from these simulations and as there is measurable proton conductivity well below $\lambda = 16$ in the SSC PFSA membrane,[17] this would indicate that such conductivity is not purely governed by connectivity, and so such a threshold is not of fundamental significance.[81] Nevertheless, connectivity of water-rich clusters will be important in maintaining high proton conductivity (i.e., > 0.1 S cm^{-1}). Another important observation from Figure 3 is that, for the particular EW and MW considered, the morphologies at all levels of hydration appear to be self-similar in shape, although the size of the water and ion containing domains is increasing. The latter effect is investigated quantitatively via the Bragg spacing in Results, section II (see Figure 10).

Figure 4 shows contour plots of water (W) bead density of an SSC PFSA system for the maximum hydration level studied, $\lambda = 16$, at fixed EW 753 and MWs varying from 9036 (Figure 4a) to 36144 g/mol (Figure 4b). In other words, the morphological structures shown in Figure 4b are generated by polymers with twice the MW of those in Figure 3d, which are in turn twice as long as those in Figure 3d, with all other factors remaining constant. For comparison, note that the upper limit of MW for chains in MD simulations published to date is about 1.5×10^4 g/mol, whereas a typical PFSA polymer has an average MW in the region of 10^5 to 10^6.[82] Our largest DPD molecules are therefore of the same order of magnitude as the lower end of the experimental MW distribution. Visual inspection of the results in Figure 4 shows that doubling the MW causes a noticeable increase in size of the ion-clustered regions, although the shape of these water-rich domains remains approximately similar (larger domains connected with much narrower channels). Continuing in this vein, Figure 5 shows contour plots of water density of the SSC PFSA system for the highest hydration level studied, $\lambda = 16$, at fixed EW 798 and MWs of 11970 (Figure 5a), 23940 (Figure 5b) and 47880 g/mol (Figure 5c). These again show a discernible increase in the size of the ion-clustered regions with increasing MW, especially for the highest MW studied (Figure 5c). Since the density of ion exchange groups has remained the same, respectively, in both Figures 4 and 5, the most likely explanation for the behavior observed is that larger MWs favor greater aggregation of the fluorocarbon backbone, due to a combination of minimization of intramolecular chain bending forces (resulting from the entropic conformational penalty in forming spherical aggregates of ionic groups) and intermolecular enthalpic repulsions between ionic groups and fluorocarbon chains, which in turn drives the formation of larger water-rich domains. These chain bending forces are similar in principle to those first introduced by Mauritz

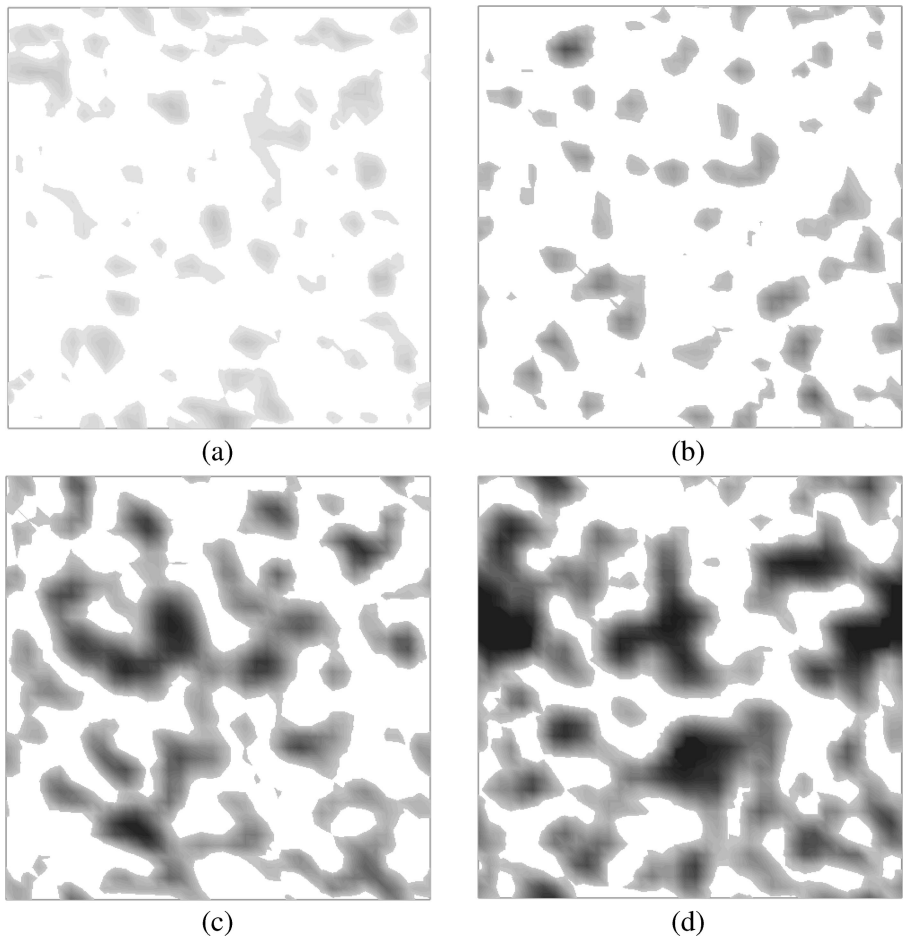

Figure 3. Contour plots of the density of the water as a two-dimensional (2D) cross section of the hydrated morphologies shown in Figure 2 (EW = 753 and MW = 18072 g/mol) at water contents of (a) 5, (b) 7, (c) 11, and (d) 16 H_2O/SO_3^-. The darkness of gray level is linearly proportional to the water density over the range from 0.00 to 3.25.

et al.[83] in their semiempirical cluster model, but whereas they calculated chain bending forces using a Gaussian coil approximation, we have used explicit polymer chains (albeit with a coarse-grained structure) in our current simulations. Furthermore, we do not assume spherical clusters, or indeed any particular model morphology, in our DPD simulations. Previous MD simulations of very low MW ionomers, in which chain bending forces are absent (e.g., Elliott et al.[84]), exhibited spherical aggregates that are rather smaller than those found experimentally in Nafion, and later MD simulations of higher MW polymers (e.g., refs 46–49).

In further support of this argument, Figure 6 also shows contour plots of water density of the SSC PFSA system for the highest hydration level studied, $\lambda = 16$, at fixed EW 849 and MWs of 17838 (Figure 6a), 35676 (Figure 6b) and 71532 g/mol (Figure 6c). As well as showing an increase in size with increasing MW, the water-rich domains also became more elongated. In particular, extended regions of low water density (white areas) appear to percolate in Figure 6c. This is again consistent with greater aggregation of the PTFE backbone material, which for higher EW polymers (i.e., those with a lower concentration of sulfonic acid groups) is sufficient to cause an elongated nonspherical aggregated structure more consistent with a fibrillar morphology, as proposed by Rubatat et al.,[32] than a spherical ion-clustered model. It is clear that the change in morphology from spherical to elongated ion clusters can be driven by increasing MW (or, more accurately, using a realistic MW comparable to real PFSA membranes) and decreasing the concentration of ionic clusters (i.e., increasing MW) due to increased aggregation of the backbone material. At this point, it is appropriate to comment on the possible effects of chain ends and entanglements. We consider that the chain lengths considered in our study (between 67−530 CF_2 repeat units) are sufficiently large that chain end effects are dominated by the side group density, which remains constant with MW. Furthermore, we consider that the cross-linking of chains due to ionomeric attachments, which occurs at a frequency of 10−30 CF_2 repeat units (depending on EW) will have a much more significant influence on the structures formed than fluorocarbon chain entanglements (which occur at the same frequency as found in PTFE, i.e., about 140 CF_2 repeat units.[85] Nevertheless, as well as considering the larger scale organization of water in the PFSA simulations, it is also instructive to quantitatively compare the distribution of water density on a more local scale using the radial distribution functions of the water beads.

II. Structural Analysis of Phase Segregated Morphologies. Figure 7 shows a comparison of the RDFs of water beads for the SSC PFSA systems at three distinct hydration levels ($\lambda = 5$, 9, and 16) for a fixed EW = 753 and MWs of 9036 (Figure 7a), 18072 (Figure 7b) and 36144 g/mol (Figure 7c). These plots provide quantitative underpinning to the qualitative results presented earlier (Figure 4) and also in the case of Figure 7a demonstrate agreement with the DPD simulations of our prior work on an SSC PFSA ionomer with EW = 678 and MW = 10170 g/mol.[68] Clearly, the hydrated morphology of this rather low EW ionomer is very similar at the low water contents and only exhibits swelling with a substantial increase in the average size of the water domains at the highest water content ($\approx$ 16 H_2O/SO_3H). The $g(r)$'s show very little differences with

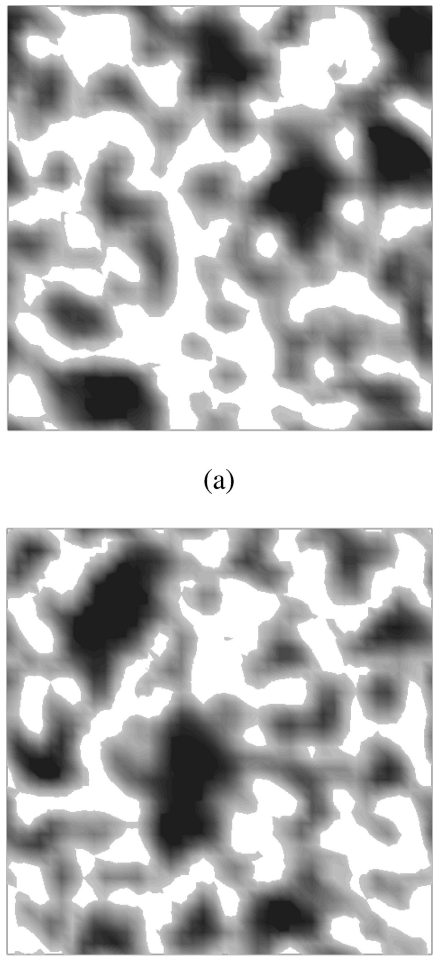

Figure 4. Contour plots of water density in a 2D cross section for the SSC PFSA ionomer at a hydration level corresponding to $\lambda = 16$ H_2O/SO_3^-: (a) EW = 753 and MW = 9036 g/mol; (b) EW = 753 and MW = 36144 g/mol.

increasing MW, regardless of water content, probably due to the high concentration of sulfonic acid groups which dominate over the effects of backbone aggregation. However, in Figure 8, there is a comparison of the RDFs of water beads for the SSC PFSA systems at the same three water contents for a fixed EW = 798 and MWs of 11970 (Figure 8a), 23940 (Figure 8b) and 47880 (Figure 8c) g/mol. These do show some differences in the first nearest neighbor peak for the two highest MWs considered (Figure 8, parts b and c). In particular, at the highest water content ($\lambda = 16$) for MW = 47880, the RDF shows a higher probability density of water beads at greater distances, which suggests slight elongation of clusters in Figure 5c. However, the effect is much more pronounced in Figure 9, which shows a comparison of the RDFs of water beads for the SSC PFSA systems at hydration levels of 5, 9, and 16 H_2O/SO_3H for fixed EW = 849 and MWs of 17838 (Figure 9a), 35676 (Figure 9b) and 71532 (Figure 9c) g/mol. For the highest MW considered, Figure 9c, the change in water density distribution for $\lambda = 16$ strongly suggests that the water domains are nonspherical.

In order to derive a measure for the relative size of the water-rich domains in Figures 4 to 7 domains, the structure factors were computed from the radial distribution functions using the procedure described in the Introduction. Figure 10 shows a comparison of the Bragg spacing, *d*, of the water peak computed from the first peak of the structure factor as a function of

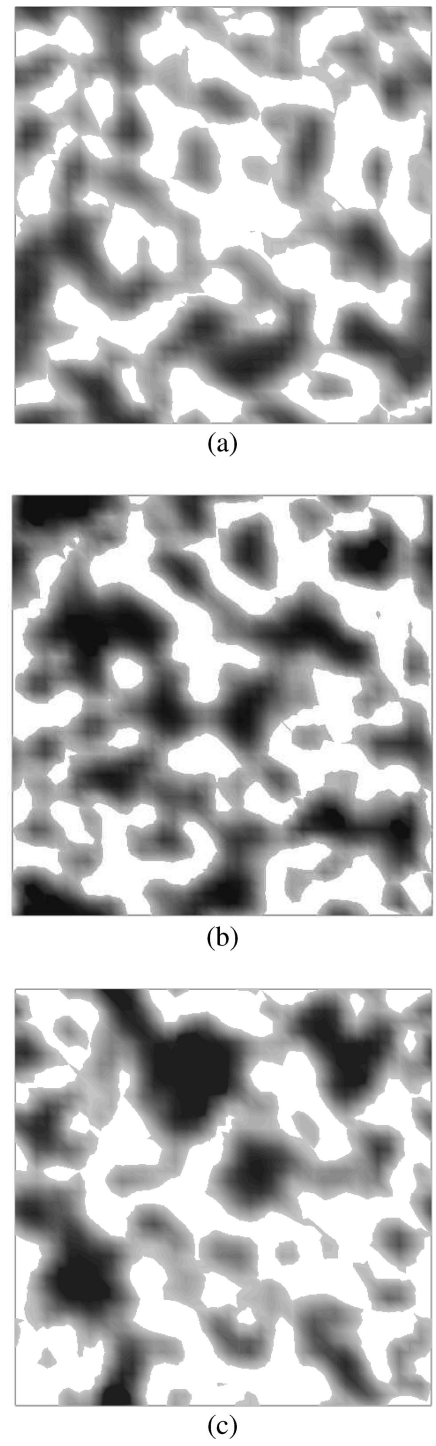

Figure 5. Contour plots of water density in a 2D cross section for the SSC PFSA ionomer at a hydration level corresponding to $\lambda = 16$ H_2O/SO_3^-: (a) EW = 798 and MW = 11970 g/mol; (b) EW = 798 and MW = 23940 g/mol; (c) EW = 798 and MW = 47880 g/mol.

hydration for three different EWs = 753 (Figure 10a), 798 (Figure 10b), and 849 (Figure 10c) as MW is increased. These show that for the two higher EWs, 798 and 849, the effect of increasing MW is to increase the average size of the water-rich domains for a given water content, whereas for the lowest EW = 753 there is only a relatively modest influence of MW. This supports the hypothesis that aggregation of the PTFE backbone becomes more dominant over the influence of ion-clustered in determining the overall morphology as MW is increased. However this difference is only manifest in the swelling data at higher water contents ($\lambda = 16$). Furthermore, it can be seen

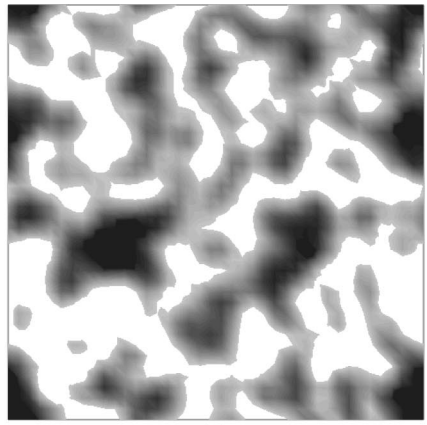

(a)

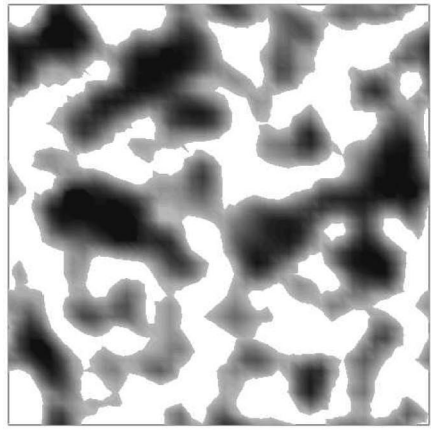

(b)

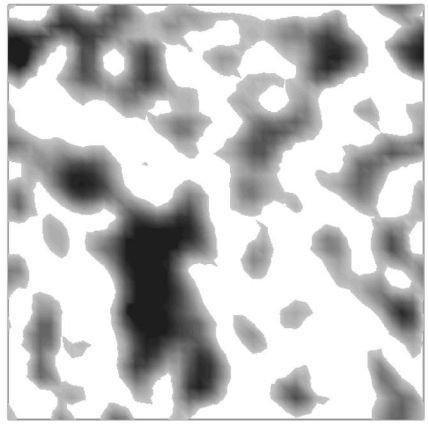

(c)

Figure 6. Contour plots of water density in a 2D cross section for the SSC PFSA ionomer at a hydration level corresponding to $\lambda = 16$ H_2O/SO_3^-: (a) EW = 849 and MW = 17838 g/mol; (b) EW = 849 and MW = 35676 g/mol; (c) EW = 849 and MW = 71352 g/mol.

from comparing Figures 4b and 6c and Figures 10a and 10c that when the ion-clustered morphology consists of nonspherical aggregates, the swelling behavior as a function of water content deviates more strongly from a linear relationship, as has been previously predicted by phenomenological swelling models.[24]

Conclusions

We have studied the swelling behavior of SSC PFSA polymer systems using DPD simulations, and found that there is a strong influence of MW on both the shape and size of water-rich ionic aggregates formed as a function of water content, particularly

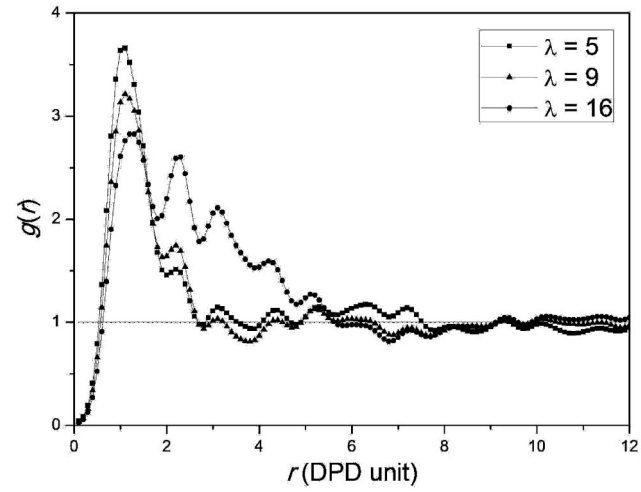

(a)

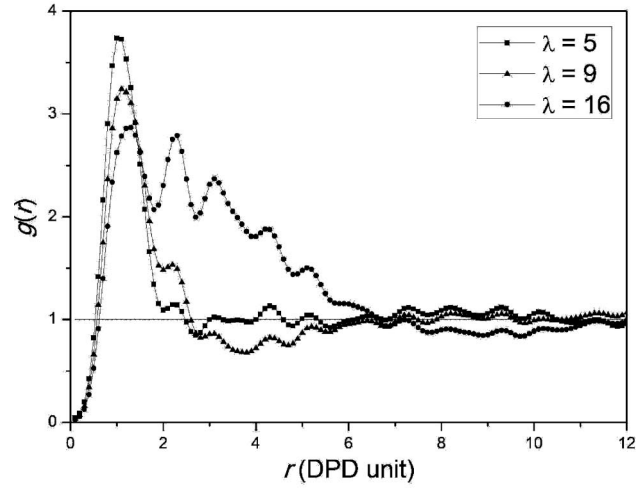

(b)

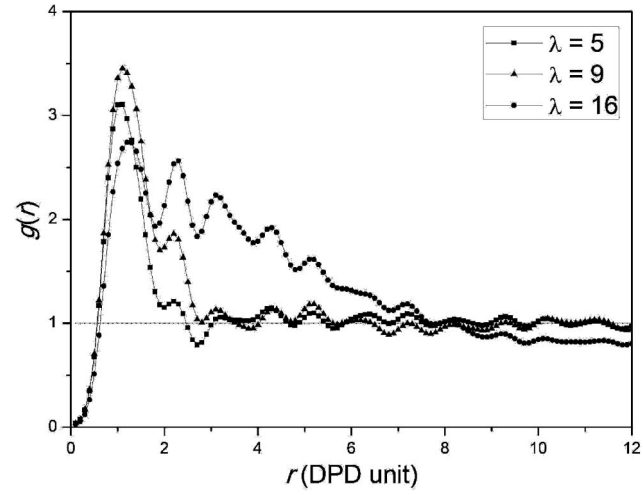

(c)

Figure 7. Radial distribution functions, $g(r)$'s, of the water particles of the SSC PFSA ionomers at various hydration levels: (a) EW = 753, MW = 9036; (b) EW = 753 and MW = 18072; and (c) EW = 753 and MW = 36144.

for high EWs where there is a low concentration of sulfonic acid groups. This is most likely due to the increased propensity for the PTFE backbone to aggregate to form fibrillar structures as the MW is increased in order to minimize total chain bending

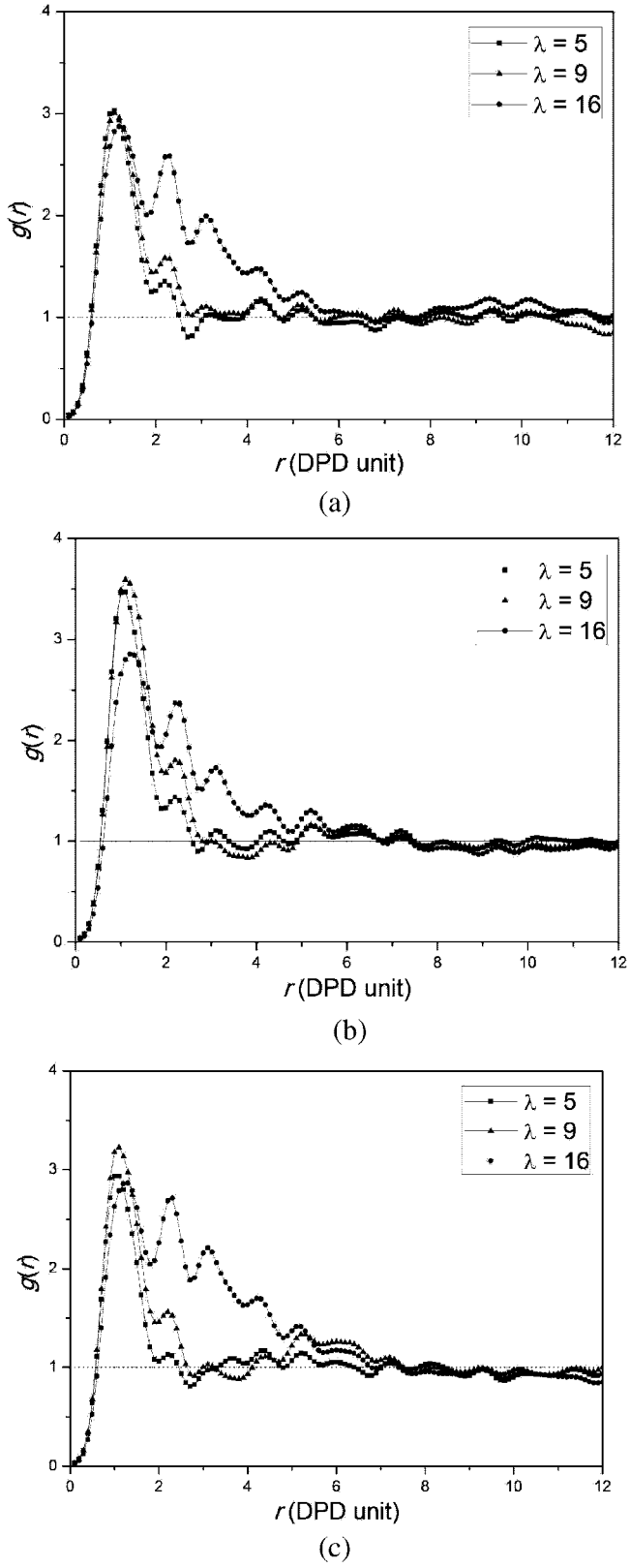

Figure 8. Radial distribution functions, $g(r)$'s, of water particles for the SSC PFSA membranes at various hydration levels: (a) EW = 798 and MW = 11970; (b) EW = 798 and MW = 23940; (c) EW = 798 and MW = 47880.

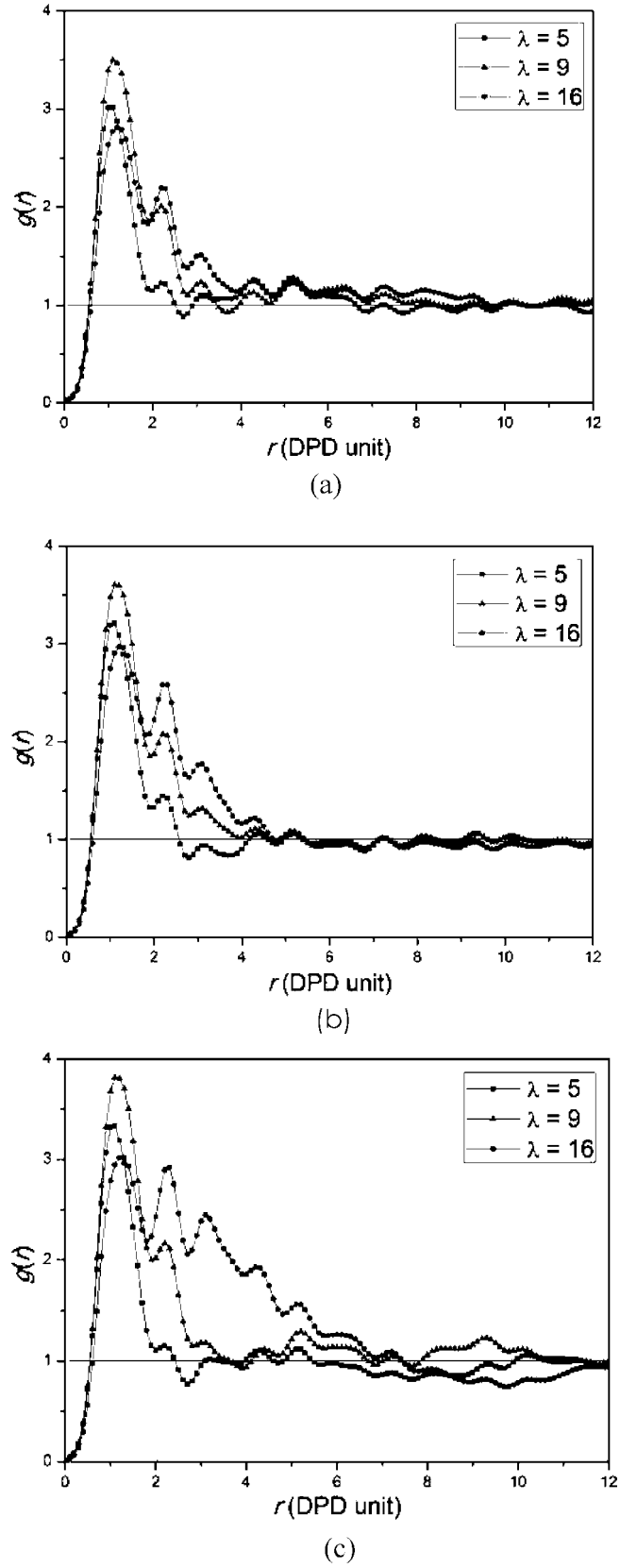

Figure 9. Radial distribution functions, $g(r)$'s, of water particles for the SSC PFSA membranes at various hydration levels: (a) EW = 849 and MW = 17838; (b) EW = 849 and MW = 35676; (c) EW = 849 and MW = 71352.

energy while maintaining phase separation between the ionic and perfluorinated components. Given that all previous molecular simulations of PFSAs have used MWs well below the values studied here, it is not surprising that these effects have not been seen previously, and that nearly all atomistic models of PFSA morphology predict spherical ion-clustered domains. Since even our largest DPD simulations still contain molecules whose MW is just below the lower limit of the MW range observed for real PFSAs, so this effect is likely to be even more

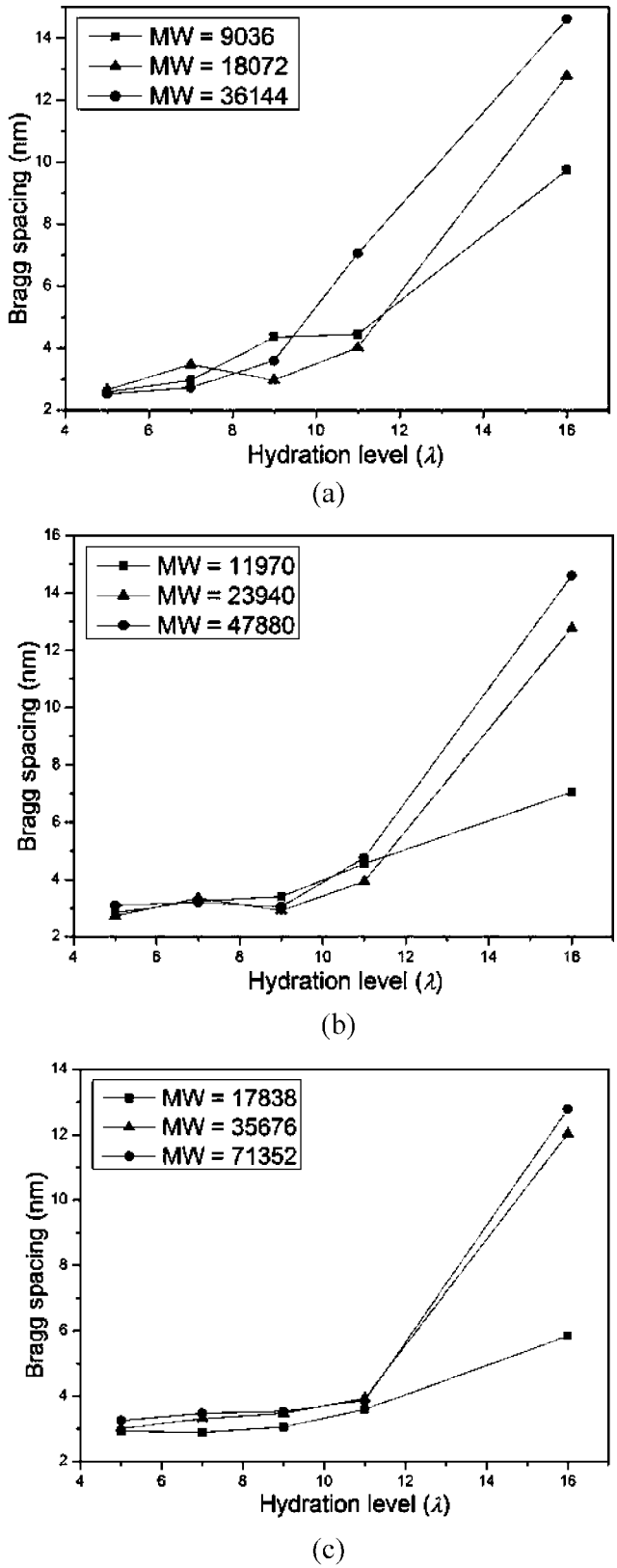

Figure 10. Bragg spacing, *d*, as a function of the hydration levels: (a) EW of 753; (b) EW of 798; (c) EW of 849.

pronounced than found here, and may be one of the reasons why there is still so much disagreement between the various different morphologies predicted for PFSAs by modeling studies. Our study has shown that MW does have a significant effect on the hydrated morphology particularly at the upper hydration limit examined in this study (i.e., $\lambda = 16$) and swelling of SSC PFSAs, and this finding is likely to be general across PFSA membranes with different side-chain length.

Acknowledgment. This work was supported by the U.S. Army Research Laboratory and the U.S. Army Research Office under Contract Number W911NF-07-1-0085.

References and Notes

(1) Hamrock, S. J.; Yandrasits, M. A. *Polym. Rev.* **2006**, *46*, 219–244.
(2) Kundu, P. P.; Pal, A. *Rev. Chem. Eng.* **2006**, *22*, 125–153.
(3) Mauritz, K. A.; Moore, R. B. *Chem. Rev.* **2004**, *104*, 4535–4585.
(4) Kreuer, K. D. *Chemphyschem* **2002**, *3*, 771–775.
(5) Savadogo, O. *J. Power Sources* **2004**, *127*, 135–161.
(6) Tant, M. R.; Lee, K. D.; Darst, K. P.; Martin, C. W. *Polym. Mater. Sci. Eng.* **1988**, *58*, 1074.
(7) Tant, M. R.; Darst, K. P.; Lee, K. D.; Martin, C. W. *ACS Symp. Ser.* **1989**, *395*, 370–400.
(8) Moore, R. B.; Martin, C. R. *Macromolecules* **1989**, *22*, 3594–3599.
(9) Prater, K. *J. Power Sources* **1990**, *29*, 239–250.
(10) Eisman, G. A. *J. Power Sources* **1990**, *29*, 389–398.
(11) Gebel, G.; Moore, R. B. *Macromolecules* **2000**, *33*, 4850–4855.
(12) Arcella, V.; Ghielmi, A.; Tommasi, G. *Ann. N.Y. Acad. Sci.* **2003**, *984*, 226–244.
(13) Ghielmi, A.; Vaccarono, P.; Troglia, C.; Arcella, V. *J. Power Sources* **2005**, *145*, 108–115.
(14) Arcella, V.; Troglia, C.; Ghielmi, A. *Ind. Eng. Chem. Res.* **2005**, *44*, 7646–7651.
(15) Merlo, L.; Ghielmi, A.; Cirillo, L.; Gebert, M.; Arcella, V. *J. Power Sources* **2007**, *171*, 140–147.
(16) Merlo, L.; Ghielmi, A.; Cirillo, L.; Gebert, M.; Arcella, V. *Sep. Sci. Technol.* **2007**, *42*, 2891–2908.
(17) Kreuer, K. D.; Schuster, M.; Obliers, B.; Diat, O.; Traub, U.; Fuchs, A.; Klock, U.; Paddison, S. J.; Maier, J. *J. Power Sources* **2008**, *178*, 499–509.
(18) Gorri, D.; De Angelis, M. G.; Giacinti Baschetti, M.; Sarti, G. C. *J. Membr. Sci.* **2008**, *322*, 383–391.
(19) Navarrini, W.; Scrosati, B.; Panero, S.; Ghielmi, A.; Sanguineti, A.; Geniram, G. *J. Power Sources* **2008**, *178*, 783–788.
(20) Ezzell, B. R.; Carl, W. P.; Mod, W. A. *4*,358,412, **1982**.
(21) Zawodzinski, T. A.; Derouin, C.; Radzinski, S.; Sherman, R. J.; Smith, V. T.; Springer, T. E.; Gottesfeld, S. *J. Electrochem. Soc.* **1993**, *140*, 1041–1047.
(22) Edmondson, C. A.; Stallworth, P. E.; Chapman, M. E.; Fontanella, J. J.; Wintersgill, M. C.; Chung, S. H.; Greenbaum, S. G. *Solid State Ionics* **2000**, *135*, 419–423.
(23) Edmondson, C. A.; Fontanella, J. J. *Solid State Ionics* **2002**, *152*, 355–361.
(24) Kumar, S.; Pineri, M. *J. Polym. Sci., Polym. Phys. Ed.* **1986**, *24*, 1767–1782.
(25) Gebel, G.; Lambard, J. *Macromolecules* **1997**, *30*, 7914–7920.
(26) Gierke, T. D.; Munn, G. E.; Wilson, F. C. *J. Polym. Sci.* **1981**, *19*, 1687–1704.
(27) Hsu, W. Y.; Gierke, T. D. *Macromolecules* **1982**, *15*, 101–105.
(28) Hsu, W. Y.; Gierke, T. D. *J. Membr. Sci.* **1983**, *13*, 307–326.
(29) Fujimura, M.; Hashimoto, T.; Kawai, H. *Macromolecules* **1981**, *14*, 1309–1315.
(30) Litt, M. H. *Polym. Prepr.* **1997**, *38*.
(31) Haubold, H. G.; Vad, T.; Jungbluth, H.; Hiller, P. *Electrochim. Acta* **2001**, *46*, 1559–1563.
(32) Rubatat, L.; Rollet, A. L.; Gebel, G.; Diat, O. *Macromolecules* **2002**, *35*, 4050–4055.
(33) Kreuer, K. D. *J. Membr. Sci.* **2001**, *185*, 29–39.
(34) Schmidt-Rohr, K.; Chen, Q. *Nat. Mater.* **2008**, *7*, 75–83.
(35) Paddison, S. J. *Annu. Rev. Mater. Res.* **2003**, *33*, 289–319.
(36) Kreuer, K. D.; Paddison, S. J.; Spohr, E.; Schuster, M. *Chem. Rev.* **2004**, *104*, 4637–4678.
(37) Elliott, J. A.; Paddison, S. J. *Phys. Chem. Chem. Phys.* **2007**, *9*, 2602–2618.
(38) Paddison, S. J.; Elliott, J. A. *J. Phys. Chem. A* **2005**, *109*, 7583–7593.
(39) Paddison, S. J.; Elliott, J. A. *Phys. Chem. Chem. Phys.* **2006**, *8*, 2193–2203.
(40) Paddison, S. J.; Elliott, J. A. *Solid State Ionics* **2006**, *177*, 2385–2390.
(41) Paddison, S. J.; Elliott, J. A. *Solid State Ionics* **2007**, *178*, 561–567.
(42) Eikerling, M.; Paddison, S. J.; Pratt, L. R.; Zawodzinski, T. A. *Chem. Phys. Lett.* **2003**, *368*, 108–114.
(43) Roudgar, A.; Narasimachary, S. P.; Eikerling, M. *J. Phys. Chem. B* **2006**, *110*, 20469–20477.
(44) Roudgar, A.; Narasimachary, S. P.; Eikerling, M. *Chem. Phys. Lett.* **2008**, *457*, 337–341.
(45) Narasimachary, S. R.; Roudgar, A.; Eikerling, M. *Electrochim. Acta* **2008**, *53*, 6920–6927.

(46) Vishnyakov, A.; Neimark, A. V. *J. Phys. Chem. B* **2000**, *104*, 4471–4478.
(47) Jang, S. S.; Molinero, V.; Cagin, T.; Goddard, W. A. *J. Phys. Chem. B* **2004**, *108*, 3149–3157.
(48) Urata, S.; Irisawa, J.; Takada, A.; Shinoda, W.; Tsuzuki, S.; Mikami, M. *J. Phys. Chem. B* **2005**, *109*, 4269–4278.
(49) Urata, S.; Irisawa, J.; Takada, A.; Shinoda, W.; Tsuzuki, S.; Mikami, M. *J. Phys. Chem. B* **2005**, *109*, 17274–17280.
(50) Blake, N. P.; Petersen, M. K.; Voth, G. A.; Metiu, H. *J. Phys. Chem. B* **2005**, *109*, 24244–24253.
(51) Blake, N. P.; Mills, G.; Metiu, H. *J. Phys. Chem. B* **2007**, *111*, 2490–2494.
(52) Venkatnathan, A.; Devanathan, R.; Dupuis, M. *J. Phys. Chem. B* **2007**, *111*, 7234–7244.
(53) Devanathan, R.; Venkatnathan, A.; Dupuis, M. *J. Phys. Chem. B* **2007**, *111*, 8069–8079.
(54) Devanathan, R.; Venkatnathan, A.; Dupuis, M. *J. Phys. Chem. B* **2007**, *111*, 13006–13013.
(55) Hristov, I. H.; Paddison, S. J.; Paul, R. *J. Phys. Chem. B* **2008**, *112*, 2937–2949.
(56) Cui, S. T.; Liu, J. W.; Selvan, M. E.; Paddison, S. J.; Keffer, D. J.; Edwards, B. J. *J. Phys. Chem. B* **2008**, *112*, 13273–13284.
(57) Dokmaisrijan, S.; Spohr, E. *J. Mol. Liq.* **2006**, *129*, 92–100.
(58) Petersen, M. K.; Wang, F.; Blake, N. P.; Metiu, H.; Voth, G. A. *J. Phys. Chem. B* **2005**, *109*, 3727–3730.
(59) Khalatur, P. G.; Talitskikh, S. K.; Khokhlov, A. R. *Macromol. Theory Simul.* **2002**, *11*, 566–586.
(60) Galperin, D. Y.; Khokhlov, A. R. *Macromol. Theory Simul.* **2006**, *15*, 137–146.
(61) Wescott, J. T.; Qi, Y.; Subramanian, L.; Capehart, T. W. *J. Chem. Phys.* **2006**, *124*, 134702.
(62) Yamamoto, S.; Hyodo, S. A. *Polym. J.* **2003**, *35*, 519–527.
(63) Malek, K.; Eikerling, M.; Wang, Q. P.; Liu, Z. S.; Otsuka, S.; Akizuki, K.; Abe, M. *J. Chem. Phys.* **2008**, *129*, 204702.
(64) Groot, R. D.; Warren, P. B. *J. Chem. Phys.* **1997**, *107*, 4423–4435.
(65) Groot, R. D.; Madden, T. J. *J. Chem. Phys.* **1998**, *108*, 8713–8724.
(66) Groot, R. D.; Rabone, K. L. *Biophys. J.* **2001**, *81*, 725–736.
(67) Grafmuller, A.; Shillcock, J.; Lipowsky, R. *Phys. Rev. Lett.* **2007**, *98*, 4.
(68) Wu, D.-S.; Paddison, S. J.; Elliott, J. A. *Energy Environ. Sci.* **2008**, *1*, 284–293.
(69) Khokhlov, A. R.; Khalatur, P. G. *Chem. Phys. Lett.* **2008**, *461*, 58–63.
(70) Hoogerbrugge, P. J.; Koelman, J. M. V. A. *Europhys. Lett.* **1992**, *19*, 155–160.
(71) Koelman, J. M. V. A.; Hoogerbrugge, P. J. *Europhys. Lett.* **1993**, *21*, 363–368.
(72) *Materials Studio, 4.1*; Accelrys Software Inc.: San Diego, CA, 2006.
(73) Español, P.; Warren, P. B. *Europhys. Lett.* **1995**, *30*, 191–196.
(74) Español, P. *Europhys. Lett.* **1997**, *40*, 631–636.
(75) Fan, C. F.; Olafson, B. D.; Blanco, M.; Hsu, S. L. *Macromolecules* **1992**, *25*, 3667–3676.
(76) Schweizer, K. S.; Curro, J. G. *J. Chem. Phys.* **1989**, *91*, 5059–5081.
(77) Frisch, M. J.; Trucks, G. W.; Schlegel, H. B.; Scuseria, G. E.; Robb, M. A.; Cheeseman, J. R.; Montgomery, J. A.; Vreven, T.; Kudin, K. N.; Burant, J. C.; Millam, J. M.; Iyengar, S. S.; Tomasi, J.; Barone, V.; Mennucci, B.; Cossi, M.; Scalmani, G.; Rega, N.; Petersson, G. A.; Nakatsuji, H.; Hada, M.; Ehara, M. ; Toyota, K.; Fukuda, R.; Hasegawa, J.; Ishida, M.; Nakajima, T.; Honda, Y.; Kitao, O.; Nakai, H.; Klene, M.; Li, X.; Knox, J. E.; Hratchian, H. P.; Cross, J. B.; Adamo, C.; Jaramillo, J.; Gomperts, R.; Stratmann, R. E.; Yazyev, O.; Austin, A. J.; Cammi, R.; Pomelli, C.; Ochterski, J. W.; Ayala, P. Y.; Morokuma, K.; Voth, G. A.; Salvador, P.; Dannenberg, J. J.; Zakrzewski, V. G.; Dapprich, S.; Daniels, A. D.; Strain, M. C.; Farkas, O.; Malick, D. K.; Rabuck, A. D.; Raghavachari, K.; Foresman, J. B.; Ortiz, J. V.; Cui, Q.; Baboul, A. G.; Clifford, S.; Cioslowski, J.; Stefanov, B. B.; Liu, G.; Liashenko, A.; Piskorz, P.; Komaromi, I.; Martin, R. L.; Fox, D. J.; Keith, T.; Al-Laham, M. A.; Peng, C. Y.; Nanayakkara, A.; Challacombe, M.; Gill, P. M. W.; Johnson, B.; Chen, W.; Wong, M. W.; Gonzalez, C.; Pople, J. A. *Gaussian 03*, Revision C.02; Gaussian Inc.: Wallingford, CT, 2004.
(78) Yoon, B. J.; Jhon, M. S.; Eyring, H. *Proc. Natl. Acad. Sci. U.S.A.* **1981**, *78*, 6588–6591.
(79) Salacuse, J. J.; Denton, A. R.; Egelstaff, P. A. *Phys. Rev. E* **1996**, *53*, 2382–2389.
(80) Salacuse, J. J.; Denton, A. R.; Egelstaff, P. A.; Tau, M.; Reatto, L. *Phys. Rev. E* **1996**, *53*, 2390–2401.
(81) Paddison, S. J. Proton Conduction in PEMs: Complexity, Cooperativity and Connectivity. In *Device and Materials Modeling in PEM Fuel Cells*, Springer-Verlag: Berlin, 2008; Vol. 113, pp 385−412.
(82) Curtin, D. E.; Lousenberg, R. D.; Henry, T. J.; Tangeman, P. C.; Tisack, M. E. *J. Power Sources* **2004**, *131*, 41–48.
(83) Mauritz, K. A.; Hora, C. J.; Hopfinger, A. J. *Polym. Prepr. (Am. Chem. Soc., Div. Polym. Chem.)* **1978**, *19*, 324.
(84) Elliott, J. A.; Hanna, S.; Elliott, A. M. S.; Cooley, G. E. *Phys. Chem. Chem. Phys.* **1999**, *1*, 4855–4864.
(85) Termonia, Y. *Polymer* **2007**, *48*, 1435–1440.

MA900016W